ChemPubSoc Europe
DOI: 10.1002/celc.201600131
CHEMELECTROCHEM
Articles

Three-Dimensional Coral-Like Structure Constructed of Carbon-Coated Interconnected Monocrystalline SnO_2 Nanoparticles with Improved Lithium-Storage Properties

Wangwang Xu, Xiaodan Cui, Zhiqiang Xie, Grant Dietrich, and Ying Wang*[a]

The applications of alloying/dealloying materials as anode for LIB electrode are hindered by its dramatic volume variations and sluggish kinetics. Herein, to overcome these challenges, we report a facile and scalable approach fabricating coral-like SnO_2/C composite electrodes through a top-down strategy followed by a sol–gel carbon-coating method. During the synthesis, well-defined SnS_2 nanoflowers and dopamine serve as structural template and carbon source for integrating the desired structure. The three-dimensional coral-like SnO_2/C composite exhibits a high reversible capacity of 648 mAh g^{-1} after 50 electrochemical cycles and a low capacity fading of 0.778 % per cycle from the 2nd to the 50th cycle, demonstrating an outstanding cycling stability. It also shows a discharge capacity of 1294, 784, 658, 532, and 434 mAh g^{-1} at a specific current of 100, 200, 500, 1000 and 2000 mAh g^{-1}, respectively, and retains a specific capacity of 719 mAh g^{-1} when the specific current goes back to 100 mA g^{-1}, displaying an excellent rate capability. Compared to SnS_2 nanoflowers and bare interconnected SnO_2 nanoparticles anode, the optimized coral-like SnO_2/C composite shows significantly improved electrochemical performances in terms of rate capability and cycling reversibility, demonstrating great potential as superior anodes in next-generation lithium ion batteries.

1. Introduction

Recently, the fast-increasing energy demand for efficient, sustainable and environmentally friendly energy storage devices has become a significant and challenging issue.[1–4] Lithium-ion batteries (LIBs) have been widely used as commercial energy devices in portable electronics and also show great promise in upcoming large-scale applications due to their advantages of environmental friendliness, safety, high efficiency and light weight.[5–7] However, to apply LIBs on large-scale machines, such as electric vehicles (EVs) and hybrid electric vehicles (HEVs), LIBs still need further improvement in capacity, energy density and stability.[8,9] Significant improvements have been achieved by exploring new electrode materials with high capacity to replace the current commercial graphite-based anodes. Recently, SnO_2-based nanostructured materials have received tremendous attention as anode materials in LIBs due to their large theoretical capacity of 781 mAh g^{-1}, which is much higher than that of current graphite anode (370 mAh g^{-1}).[10–17] Unfortunately, their practical applications in LIBs are still greatly hindered by their poor cycling stability and inferior rate capability due to severe electrode pulverizaiton and loss of interparticle contact caused by drastic volume expansion/contraction associated with the Li^+ insertion and extraction process.[14,18,19]

In the past few years, to solve the above-mentioned problem of SnO_2-based electrodes, many research efforts have been focused on fabricating various nanostructures with better structural stability, which can effectively accommodate the large volume changes upon cycling and shorten Li-ion diffusion distance, thereby leading to increased reversible capacity and improved rate capability.[20–23] Among all these studies, two effective strategies have been widely practiced. One approach is to fabricate low-dimensional nanostructured SnO_2, such as two-dimensional nanosheets, one-dimensional nanorods/nanotubes/nanowires and zero-dimensional nanoparticles, to withstand mechanical strain during lithium ion insertion/desertion.[24–27] It is believed that low-dimensional SnO_2, especially nanoparticles can interact with lithium ions more efficiently due to the large specific surface area and short pathways for electron and lithium ion transportation. For example, as reported by Pol et al., 9 nm SnO_2 nanoparticles exhibit a high specific capacity of 778 mAh g^{-1} at 0.1 C, which is close to their theoretical discharge capacity of 781 mAh g^{-1}.[28] The other strategy is coating SnO_2 with a stable inactive component, such as amorphous carbon, as a physical scaffold to buffer the serious volume change and protect active materials from direct exposure to electrolyte. Due to better electrical conductivity, amorphous carbon is usually used as a passive agent and the carbon-coated SnO_2 demonstrates much better electrochemical performance. However, either strategy can only realize enhanced electrochemical performance of SnO_2-based electrode in one aspect. Combination of the two afore-

---

[a] W. Xu, X. Cui, Z. Xie, G. Dietrich, Prof. Y. Wang
Department of Mechanical & Industrial Engineering
Louisiana State University
1416 Patrick F. Taylor Hall
Baton Rouge, LA 70803 (USA)
ywang@lsu

Supporting Information for this article can be found under http://dx.doi.org/10.1002/celc.201600131.

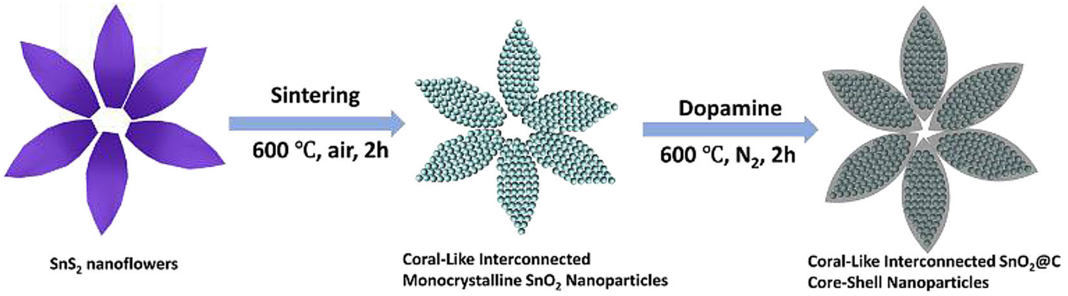

Figure 1. Synthesis of coral-like carbon-coated SnO_2/C nanoparticles.

mentioned strategies may alleviate the volume change during cycling and improve charge transport at the same time. Therefore, it would be meaningful to design and synthesize a novel SnO_2/C nanostructure.

In this work, we report a novel SnO_2/C composite nanostructure, namely, three-dimensional coral-like structures constructed by interconnected monocrystalline-SnO_2/carbon nanoparticles prepared via a facile and scalable top-down approach followed by a sol-gel carbon coating method. The synthesis procedure is mainly composed of four steps as illustrated in Figure 1. In step I, SnS_2 nanoflowers were prepared by a facile solvothermal method. In step II, the as-prepared SnS_2 nanoflowers were annealed in air to form coral-like SnO_2 nanostructures. In step III, the coral-like SnO_2 nanostructures were coated with poly-dopamine via a one-step in situ polymerization reaction of dopamine. Notably, as a nature-inspired biomimetic material with functional groups of catechol and amine, dopamine can be utilized to deposit an adhesive polydopamine film virtually on any surface by spontaneous oxidative polymerization. Compared with widely used graphene oxide (GO),[29–31] organic chemicals,[32] or polymer, dopamine is an excellent carbon source for surface modification because of the strong adhesion and controllable thickness of the resulting coating. In step IV, the coral-like SnO_2/C nanoparticles were obtained after carbonization. In this structure, the core is coral-like SnO_2 nanostructure, with a carbon shell uniformly coating on the surface. It is interesting to note that the coral-like SnO_2 nanostructure is composed of small nanoparticles subunit structure, which are interconnected by grain boundary and form the frame of the coral. There are several unique properties of coral-like carbon-coated SnO_2/C nanoparticles as Li-ion battery anode material: 1) The zero-dimensional SnO_2 nanoparticles provide more active reaction sites and offer shorter diffusion pathways due to the large exposed surface area. 2) The coral-like interconnected nanostructure can effectively prevent aggregation of small nanoparticles. More importantly, the facile strain relaxation in the interconnected nanoparticles allows them to grow in size without cracking, and thus alleviates mechanical stress between nanoparticles during lithium ion insertion/extraction. 3) The carbon layer serve as a protection shell for SnO_2 nanoparticles to accommodate drastic volume variations and alleviate disintegration and pulverization during lithiation/delithiation. Furthermore, the interconnected nanoparticles and continuous carbon layer form an integrated electron transport, leading to facile reaction kinetics with faster switching speed. To our knowledge, it is the first report of achieving the coral-like structure constructed by interconnected monocrystalline-SnO_2/C nanoparticles.

2. Results and Discussion

Figure 1 presents a schematic showing the overall synthesis procedure and the corresponding structural changes between each step. To fabricate the coral-like SnO_2/C composite, SnS_2 nanoflowers are prepared using a solvothermal method with the precursors of tin chloride and thioacetamide, firstly. The formation mechanism of SnS_2 nanoflowers may be attributed to the Ostwald ripening mechanism and self-assembly mechanism.[33] Then, different types of tin-based compounds were obtained via annealing in different atmosphere. After SnS_2 nanoflowers were sintered in argon at 600 °C for 2 h, the uniform interconnected Sn_2S_3 nanoparticles are obtained (Figure S1). Meanwhile, when SnS_2 nanoflowers were sintered in air, SnS_2 nanoflowers were oxidized into the interconnected SnO_2 nanoparticles via the following Reaction (1):

$$SnS_2 + 3\,O_2\ (g) \rightarrow SnO_2 + 2\,SO_2\ (g) \qquad (1)$$

Owing to the gas emission during this process, many interconnected pores are created in the nanoflowers, which lead to a high surface area. As a result, more active sites and shortened lithium diffusion distance are provided. Additionally, such porous structures provides void for facile stress relaxation in lithium insertion/deinsertion. With the void space in it, the nanoflowers are converted to interconnected nanoparticles, while the resultant interconnected SnO_2 nanoparticles still preserves the shape of nanoflowers, forming coral-like interconnected SnO_2 nanoparticles. Afterwards, the interconnected SnO_2 nanoparticles were coated with uniform dopamine layer by in situ polymerization. After sintering in nitrogen atmosphere at 600 °C for 2 h, coral-like carbon-coated SnO_2/C nanoparticles were obtained by carbonization of polydopamine. The crystal structures of the SnS_2 nanoflowers and the coral-like carbon-coated SnO_2/C nanoparticles were determined by XRD, as shown in Figures 2a,b. It is found that the diffraction peaks of SnS_2 nanoflowers can be identified as hexagonal tin sulfide with the lattice parameters $a = 3.638$ Å, $b = 3.638$ Å, $c = 5.88$ Å, P-3m1 space group, which is in good agreement with

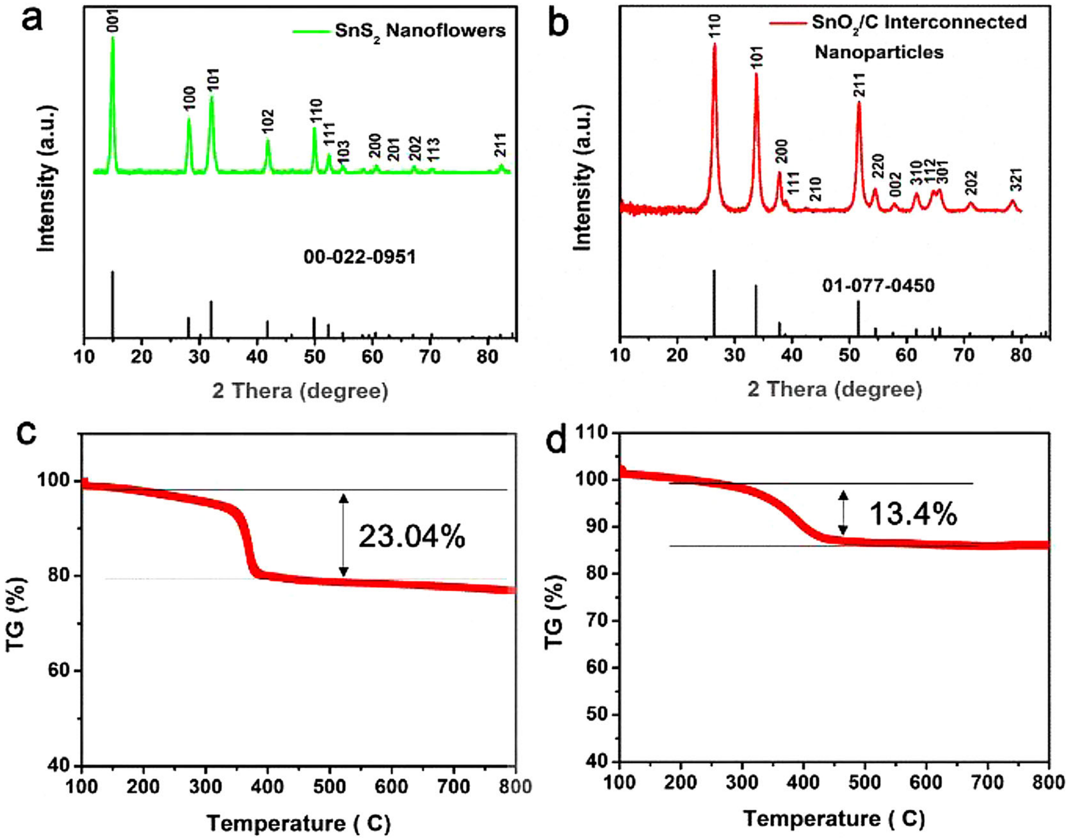

Figure 2. XRD patterns of a) SnS_2 nanoflowers, and b) coral-like carbon-coated SnO_2/C interconnected nanoparticles. TG analysis of c) SnS_2 nanoflowers and d) coral-like SnO_2/C nanoparticle

standard XRD patterns of hexagonal berndtite SnS_2 (JCPDF card no.00-022-0951). The diffraction peaks of coral-like SnO_2/C nanoparticles can be indexed to tetragonal SnO_2 with lattice parameters of $a=4.7421$ Å, $b=4.7421$ Å, $c=3.1901$ Å, P42/mnm space group, which matches well with standard XRD patterns of tetragonal rutile SnO_2 (JCPDF card no. 01-77-0450). Thermogravimetry (TG) measurements were also performed to further investigate the oxidation degree of SnS_2 and the content of carbon in the coral-like carbon-coated SnO_2/C nanoparticles. Figure 2c displays the TG curves of SnS_2 nanoflowers in air from 100 to 800 °C. It can be seen that combustion of SnS_2 nanoflowers starts at around 250 °C and is completed at approximately 425 °C. The calculated weight loss of 23.04 % is attributed to the oxidation process of SnS_2 into SnO_2 nanoparticles via Reaction (1) above. Figure 2d shows the TG curve of coral-like carbon-coated SnO_2/C nanoparticles in air. It is found that combustion of carbon starts at about 300 °C and is completed at 450 °C, corresponding to a 13.4 % weight loss of carbon in the sample during the combustion.

Figure 3 presents SEM images of the as-prepared SnS_2 nanoflowers, SnO_2 interconnected nanoparticles, and coral-like SnO_2/C nanoparticles along with the corresponding energy dispersive spectroscopy (EDS) mapping results. The low-magnification FE-SEM image of SnS_2 nanoflowers in Figure 3a reveals a flower-like morphology assembled by distinctive smooth nanosheets with lateral sizes of ~5 μm and thickness of about 10–20 nm. The nanosheet morphology is mainly caused by intrinsic anisotropic growth of SnS_2 crystals. With high uniformity and large lateral size as well as thin thickness, SnS_2 nanoflowers can serve as the precursor for preparing interconnected SnO_2 nanoparticles through sintering. After sintering in air at 600 °C for 2 h, the SnS_2 nanoflowers are converted to interconnected SnO_2 nanoparticles. As shown in the low-magnification FESEM images of the resultant SnO_2 nanoparticles (insert of Figure 3b), the flower-like morphology of SnS_2 is mostly maintained.. But unlike the SnS_2 nanoflowers, these structures are composed of many interconnected nanoparticles (Figure 3b). The diameter of these SnO_2 nanoparticles is about 50 nm. All the nanoparticles are interconnected with each other, forming the flower shape with self-organized SnO_2 "nanosheets" at the micron scale. Figure S2 and Figure 3c show FESEM images of coral-like SnO_2/poly-DPA nanoparticles and coral-like SnO_2/C nanoparticles, respectively. It is observed in Figure S2 that the uniform and smooth poly-DPA layer is coated on SnO_2 nanoparticles coherently, which may be attributed to the fact that DPA can be attached to many types of surfaces with strong interaction with the substrate.[34] After sintering in nitrogen at 600 °C for 2 h, the poly-DPA layer was carbonized in situ on the surface of SnO_2 nanoparticles. The interconnected SnO_2 nanoparticles were coated uniformly with carbon layers, forming a coral-like SnO_2/C composite material. EDS elemental mapping was performed on the coral-like SnO_2/C sample of Fig-

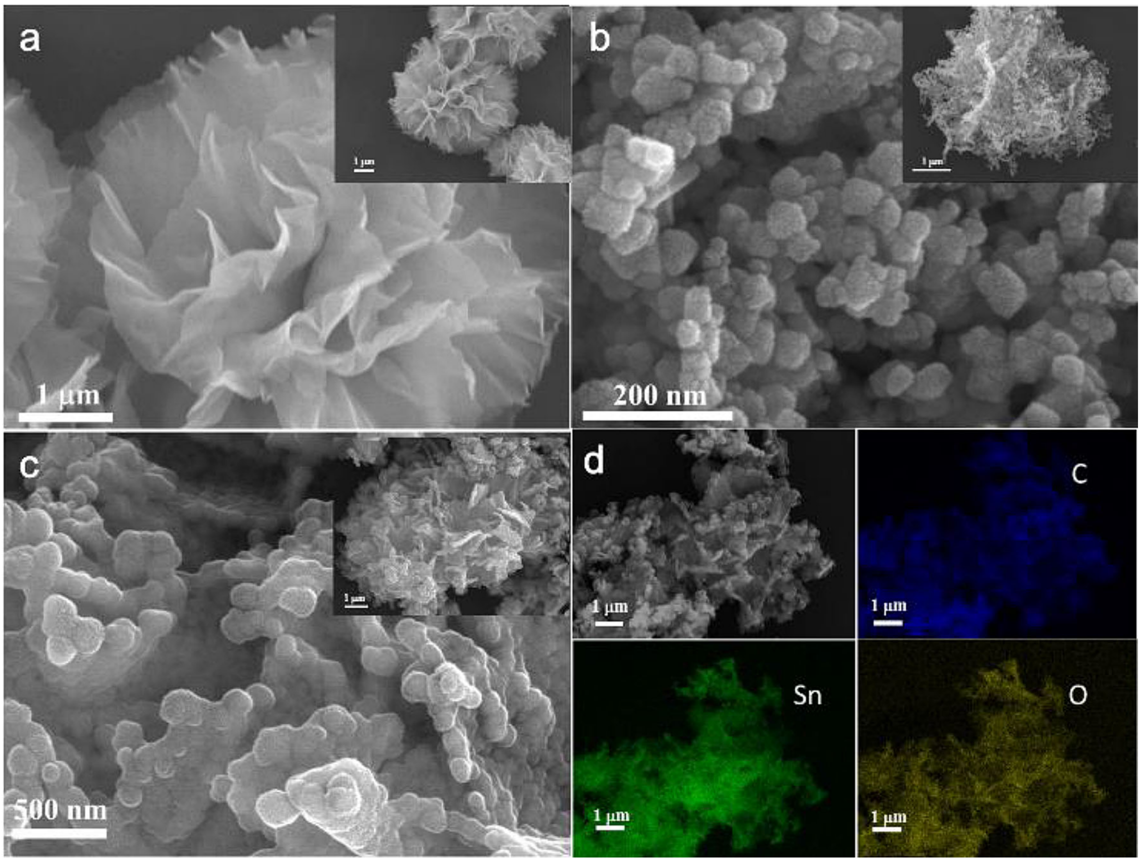

Figure 3. SEM images of a) SnS_2 nanoflowers, b) SnO_2 interconnected nanoparticles, and c) coral-like carbon-coated SnO_2/C interconnected nanoparticles, d) EDS elemental mapping of C, Sn, and O from coral-like carbon-coated SnO_2/C interconnected nanoparticles.

ure 3d. The carbon signal from carbon layer as well as the oxygen and tin signals from SnO_2 overlap uniformly across the entire sample, indicating uniform carbon coating on the surface of SnO_2 nanoparticles. Moreover, in order to examine and compare specific surface area of all the samples, the N_2 adsorption–desorption measurements are perfomed. The coral-like SnO_2/C composite material displays a BET surface area of 22.3 m^2g^{-1}, higher than that of SnS_2 nanoflowers (16.9 m^2g^{-1}) and interconnected SnO_2 nanoparticles (17.9 m^2g^{-1}).

Figure 4 presents XPS spectra of the as-prepared coral-like SnO_2/C nanoparticles. The XPS survey spectra in Figure 4a reveals the presence of tin, oxygen, nitrogen and carbon in coral-like carbon-coated SnO_2/C interconnected nanoparticles. Figure 4b–d present the high-resolution XPS spectra of C 1s, Sn 3d and N 1s, respectively. In Figure 4b, it can be seen that the C 1s region exhibits three main contributions: the peak at 284.7 eV assigned to C–C sp^2 (sp^2-hybridized graphite-like carbon), the peak at 285.5 eV that belongs to C–C sp^3 (sp^3-hybridized diamond-like carbon), the peak at 284.7 eV indicating the presence of C–O bonds, which further confirms the adhesive carbon coating. In Figure 4c, it is understood that the final products give a Sn $3d_{5/2}$ peak at 487.0 eV and a Sn $3d_{3/2}$ peak at 495.5 eV, with an energy difference of 8.5 eV, proving the existence of Sn^{4+}. In Figure 4d, the high-resolution N 1s spectrum has two major components centered at 398.4 eV and 400.3 eV, respectively, corresponding to pyridinic nitrogen and pyrrolic nitrogen, confirming the presence of nitrogen in the carbon layer. Moreover, the nitrogen content on the surface of coral-like SnO_2/C nanoparticles is calculated to be 9.48 wt% according to the X-ray photoelectron spectroscopy. These findings confirm that nitrogen from dopamine is doped into carbon during the synthesis. According to the literature,[35,36] N-doping can effectively enhance electrical conductivity of carbon coating, which facilitates charge transport in the electrode. In order to further identify the hierarchical structure of the as-prepared samples, TEM and HR-TEM coupled with electron diffraction characterizations are carried out. Figure 5a presents a TEM image of SnS_2 nanoflowers, confirming they are composed of smooth nanosheets. The HR-TEM image of nanosheets in Figure 5b exhibits lattice fringes with different d-spacings of 3.16 and 5.89 Å, corresponding to the (100) and (001) planes of hexagonal SnS_2 crystals. In addition, the TEM image of coral-like SnO_2/C nanoparticles in Figure 5c reveals the coral-like morphology is composed of interconnected SnO_2 nanoparticles coated by a uniform carbon layer with a thickness of about 13 nm, confirming the hierarchical structure. The inserted low magnification TEM image indicates that the whole SnO_2 interconnected nanoparticles framework is well coated with a carbon layer, forming integrate coral-like carbon-coated SnO_2/C interconnected nanoparticles. The HRTEM image of the nanoparticles in Figure 5d reveals lattice fringes in the SnO_2 nanoparticles with spacings of 3.35 and 3.21 Å, corresponding

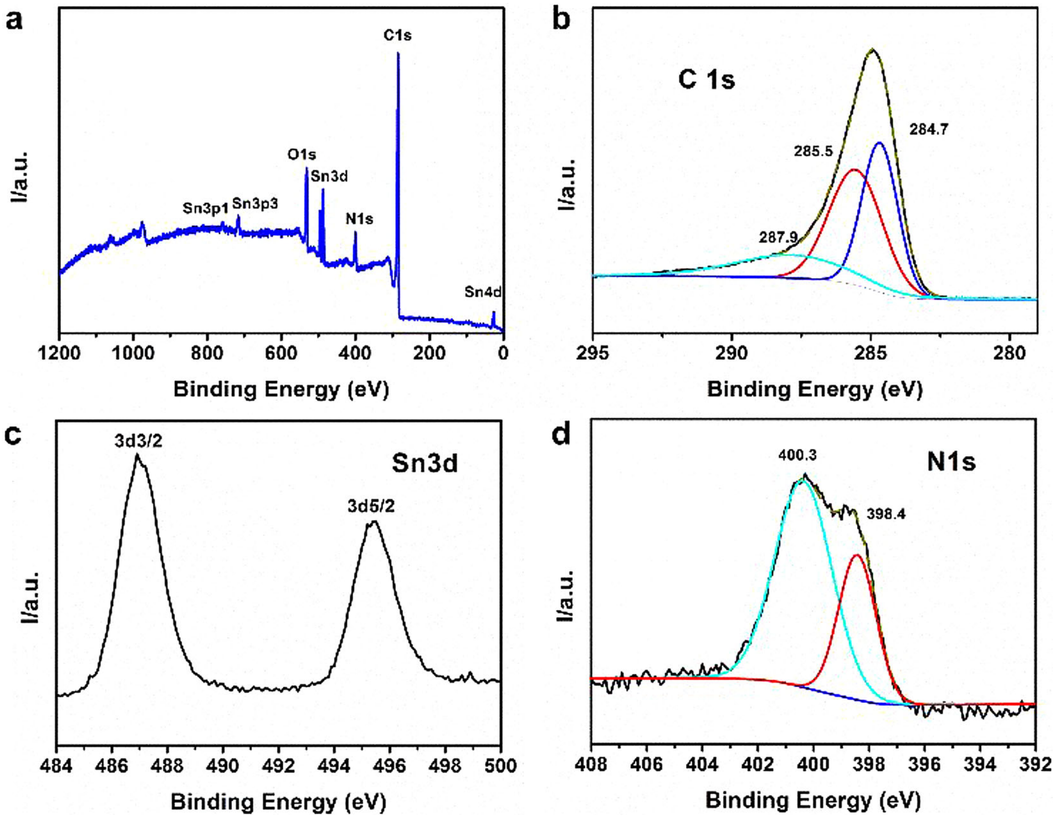

Figure 4. a) XPS survey spectrum of coral-like carbon-coated SnO_2/C interconnected nanoparticles. b) C 1s XPS spectrum, c) Sn 3d XPS spectrum, d) Sn 3d XPS spectrum of coral-like carbon-coated SnO_2/C interconnected nanoparticles.

to (101) and (001) planes of tetragonal SnO_2 crystal. Meanwhile, a SAED pattern of the same sample (inset in Figure 5 c) is well indexed as a polycrystalline hexagonal SnO_2 phase.

To investigate the electrochemical performances of all the samples, coin cells based on SnS_2 nanoflowers, SnO_2 interconnected nanoparticles, coral-like SnO_2/C composite are cycled in a voltage range of 0.01–2 V versus Li^+/Li. The electrochemical reactions of SnO_2 and SnS_2 with lithium are described below in Reactions (2)–(4):[28,37]

$$SnO_2 + 4\,Li \rightarrow 2\,Li_2O + Sn \tag{2}$$

$$SnS_2 + 4\,Li \rightarrow 2\,Li_2S + Sn \tag{3}$$

$$Sn + x\,Li^+ + xe^- \rightarrow Li_xSn \tag{4}$$

Reactions (2) and (3) are regarded as partially reversible. Therefore, theoretical capacities of SnO_2 and SnS_2 are determined to be 782 and 650 mAh g^{-1}, respectively, based on Reaction (4). Figure S3 and Figure 6 a show cyclic voltammograms (CVs) of SnS_2 nanoflowers and coral-like SnO_2/C composite in the first three consecutive cycles at a voltage range of 0.05–2 V vs. Li/Li^+. The CV curves of SnS_2 nanoflowers in Figure S3 exhibits three characteristic peaks at 1.7, 1.2 and 0.1 V in the first potential sweeping cycle, which are attributed to lithium intercalation of SnS_2 layers without phase decomposition, decomposition of SnS_2 into metallic Sn and Li_2S [Reaction (3)] and generation of a Li–Sn alloy, respectively. In subsequent cycles, the redox peaks at 0.1 V in the anodic reaction and at 0.6 V in the cathodic reaction can be ascribed to the reversible alloying and dealloying reactions of Sn and Li [Reaction (4)], respectively. Figure 6 a displays CV curves of coral-like SnO_2/C nanoparticles, showing two characteristic peaks at 0.9 and 0.1 V in the first potential sweeping cycle, which are ascribed to decomposition of SnO_2 into metallic Sn and Li_2O [Reaction (3)] and generation of a Li–Sn alloy [Reaction (4)], respectively. It is noted that the decomposition reaction is partially reversible. In subsequent cycles, intercalation of lithium ions occurs at 0.1 V and deintercalation of lithium ions occurs at 0.5 V vs. Li/Li^+, due to the alloying/dealloying reactions [Reaction (4)]. Additional cathodic peak at 0.9 V and anodic peak at 1.3 V can be attributed to the partially reversible conversion process [Reaction (2)]. This cathode and anodic pair (0.1 V, 0.5 V) is much more pronounced than the second one (0.9 V, 1.3 V), confirming the major capacity contribution of the cell. Figure 6 b shows the charge/discharge characteristics of coral-like SnO_2/C nanoparticles between 0.01 and 2.0 V vs. Li/Li^+ at a specific current of 100 mA g^{-1}. The first discharge and charge capacities of coral-like SnO_2/C nanoparticles are about 1195 and 826 mA h g^{-1}. The potential plateaus at 1.3 and 0.9 V are ascribed to the conversion reaction [Reaction (2)] between SnO_2 and Li^+, leading to the formation of Li_2O and Sn in the first discharge process. The following profiles with long slope indicate generation of Li–Sn alloy [Reaction (4)]. Such CV behavior and

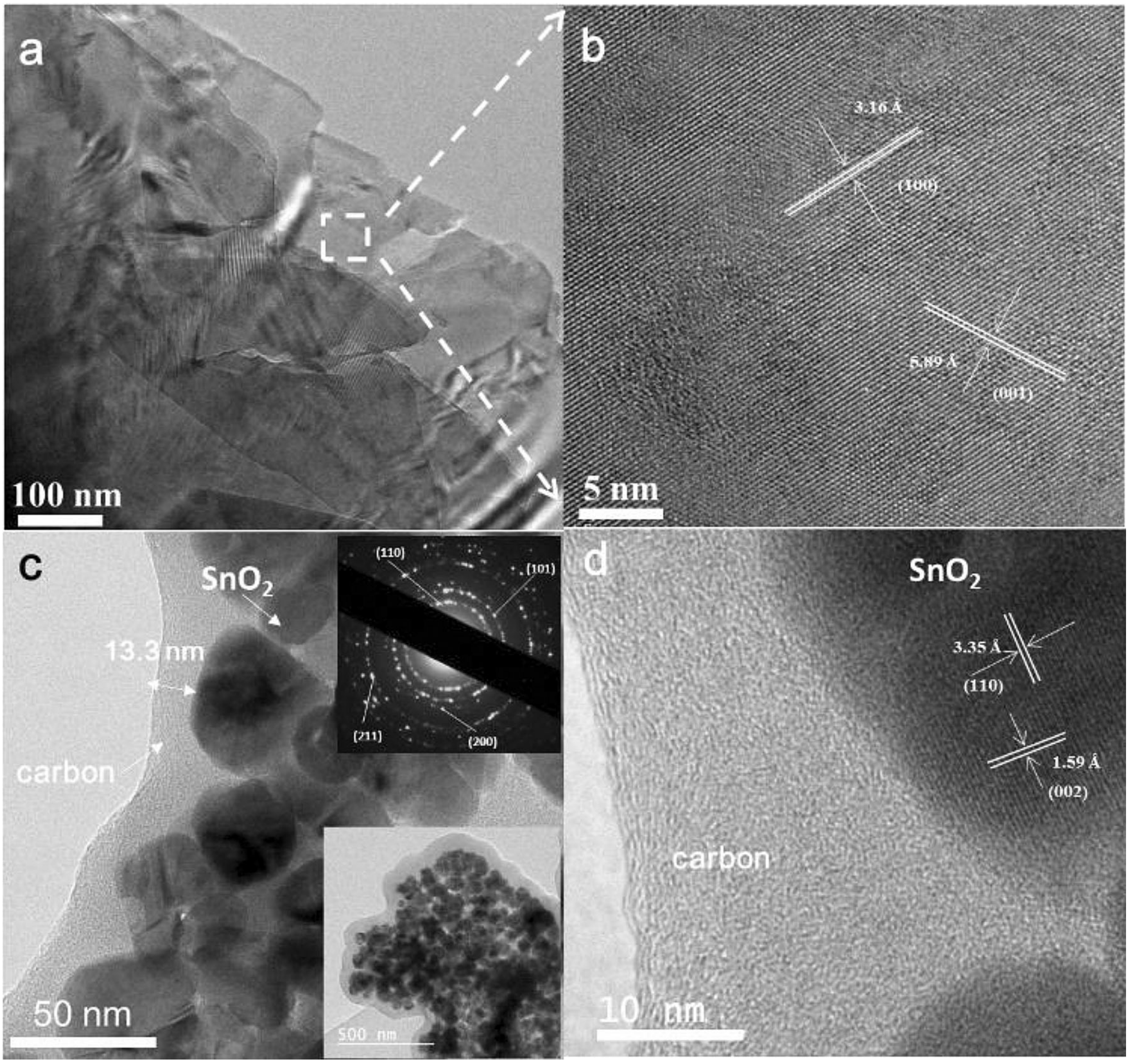

Figure 5. a) TEM image and b) HRTEM image of SnS_2 nanoflowers, c) TEM image (Inset is SAED and TEM image inlow magnification) and d) HRTEM image of coral-like SnO_2/C interconnected nanoparticles.

charge–discharge curves are generally consistent with those reported in literature.[38–40]

Figure 6 c,d summarize cycling performances of SnS_2 nanoflowers, interconnected SnO_2 nanoparticles, and coral-like SnO_2/C composite at a specific current of 200 and 500 mA g^{-1}, respectively. It is found in Figure 6 c that the initial discharge capacity of coral-like SnO_2/C composite is as high as 1280 mAh g^{-1}. However, rapid capacity decaying is observed for all the three samples, which is mainly due to partial reversibility of above-mentioned Reactions (2) and (3), and the generation of solid electrolyte interface (SEI) associated with decomposition of electrolyte.[41,42] After 50 electrochemical cycles, coral-like SnO_2/C composite maintains a capacity of 648 mAh g^{-1}, corresponding to a capacity fading of 0.778 % per cycle from the 2nd to the 50th cycle, demonstrating a large discharge capacity and good cycling stability. In contrast, drastic capacity fading is observed for interconnected SnO_2 nanoparticles after 50 cycles, corresponding to a capacity fading of as high as 1.86 % per cycle from the 2nd to 50th cycle. This result may be caused by expansion/contraction of interconnected SnO_2 nanoparticles during charge/discharge, leading to severe pulverization and delamination from the conductive substrate. Meanwhile, SnS_2 nanoflowers exhibit a lower initial discharge capacity of about 812 mAh g^{-1} and maintains a capacity of 480 mAh g^{-1} after 50 cycles, corresponding to a capacity fading as high as 1.19 % per cycle from the 2nd to the 50th cycle, which may be attributed to the lower theoretical capacity and fewer active sites of SnS_2 nanoflowers. When the specific current is increased to 500 mA g^{-1}, the coral-like SnO_2/C composite exhibits more distinct enhancement in cycling performance compare to the other two. As shown in Figure 6 d, coral-like SnO_2/C composite delivers a discharge capacity of 520 mAh g^{-1} after 50 cycles, in comparison with 345 mAh g^{-1} from interconnected SnO_2 nanoparticles and 206 mAh g^{-1} from SnS_2 nanosheets. A slight decay at the end of the 50th cycle of coral-like SnO_2/C composite is attributed to a certain extent of polarization at a high specific current. Compared to interconnected SnO_2 nanoparticles and SnS_2

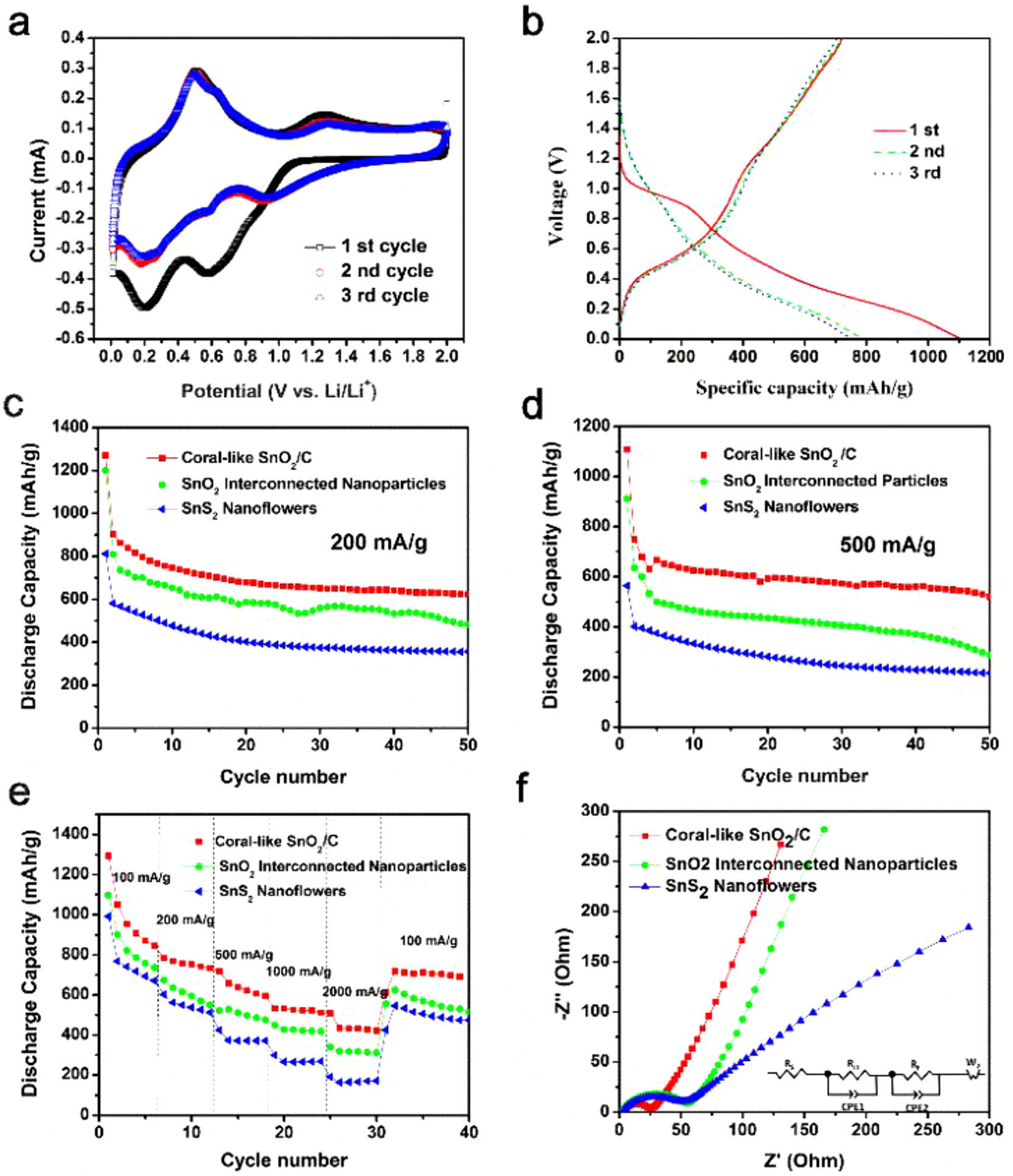

Figure 6. a) CV curves and b) galvanostatic charge-discharge profiles of the first three cycles of coral-like SnO_2/C nanoparticles. c,d) Cycling performances of hierarchical SnS_2 nanoflowers, SnO_2 interconnected nanoparticles, coral-like SnO_2/C nanoparticles at a specific current of 200 and 500 mAh g^{-1}, respectively. e) Rate performances of SnS_2 nanoflowers, SnO_2 interconnected nanoparticles, coral-like SnO_2/C nanoparticles at the specific current ranging from 100, 200, 500, 1000, 2000 to 100 mA g^{-1}; f) Nyquist plots of SnS_2 nanoflowers, SnO_2 interconnected nanoparticles, coral-like SnO_2/C nanoparticles at 100% depth.

nanosheets, coral-like SnO_2/C composite anode displays larger discharge capacity and better cycling ability, which is attributed to the unique composite structure with more electron transport pathways, more active sites and better mechanical integrity. Mechanical integrity of coral-like SnO_2/C composite is verfied by SEM images of the electrode that has been cycled for 50 cycles at 200 mA g^{-1} (Figure S4). It can be seen that the coral-like SnO_2/C composite can maintain its integral coral-like structure with the carbon layer firmly attached, since the continuous carbon layer coated on SnO_2 nanoparticles can not only effectively release the stress of volume expansion and maintain mechanical integrity during cycling, but also promote continuous electron transport and prohibit the formation of SEI film.

The rate performances of all three samples are summarized in Figure 6e. Coral-like SnO_2/C composite delivers a discharge capacity of 1294, 784, 658, 532, and 434 mAh g^{-1} at specific currents of 100, 200, 500, 1000 and 2000 mA g^{-1}, respectively. When the specific current goes back from 2000 to 100 mA g^{-1}, the discharge capacity of coral-like SnO_2/C electrode is recovered to 719 mAh g^{-1}, showing better rate capability than the interconnected SnO_2 nanoparticles (625 mAh g^{-1}) and SnS_2 nanoflowers (546 mAh g^{-1}). This is due to the good mechanical integrity of hierarchical structure during fast lithium intercalation/deintercalation process. Moreover, carbon layer firmly coated on SnO_2 nanosheets provides a continuous pathway for fast electron transport, as confirmed by the results of electrochemical impedance spectroscopy (EIS) in Figure 6 f. EIS technology is used to investigate the processes occurring at the electrode/electrolyte interfaces and Li^+ intercalation/deintercalation within electrode materials in the battery cells.[43] In the Nyquist plots, R_Ω represents the Ohmic resistance of the battery cell, including electrodes, electrolyte and other cell components. R_{ct} represents the charge transfer resistance. CPE and Z_w are the double-layer capacitance and the Warburg impedance, respectively. The Nyquist plots of all the three electrodes are composed of a depressed semicircle in the medium-frequency region followed by a slanted line in the low-frequency region. The electrode of coral-like SnO_2/C composite shows the lowest charge transfer resistance of 25 Ω compared to interconnected SnO_2 nanoparticles (55 Ω) and the SnS_2 nanoflowers (50 Ω), indicating faster charge transfer at the electrode/electrolyte interface. Additionally, in comparison with the SnS_2 nanoflowers, the slope of the plot from interconnected SnO_2 nanoparticles and coral-like SnO_2/C composite increases distinctly at the low-frequency range, suggesting that the R_{ct} values for the interconnected SnO_2 nanoparticles and the coral-like SnO_2/C composite are much lower than those of SnS_2 nanoflowers. These results may be attributed to larger surface area and more active sites of interconnected SnO_2 nanoparticles and coral-like SnO_2/C composite. Moreover, the identical slope of the EIS plots for the interconnected SnO_2 nanoparticles and coral-like SnO_2/C composite indicates that the carbon coating on the surface of SnO_2 does not hinder transportation of lithium ions. In order to investigate structural stability of the designed coral-like SnO_2/C composites, the charge transfer resistances of the electrodes after electrochemical cycling are analyzed. Figure S5 compares Nyquist plots of the coral-like SnO_2/C composite cells before and after 50 cycles when cycled at 200 $mA\,g^{-1}$. In comparison with the cell before cycling, the cell after cycling shows a slight increase of R_Ω resistance to 48.0 Ω and a similar slope of the slanted line, demonstrating stable kinetics of electrochemical reactions in the battery cell based on coral-like SnO_2/C composite.

The improved rate capability and cycling reversibility of the as-prepared coral-like SnO_2/C composite might be owing to novel engineering and design of its interconnected nanostructure and composition. Due to the overall coral-like microstructure and ultrasmall nanoparticle subunits as well as soft carbon shell, the coral-like SnO_2/C composite displays much higher capacity than SnS_2 and pure SnO_2 electrodes, especially at high specific current. Specifically, the coral-like frame structure and ultrasmall nanoparticle subunits possess short pathways for transportation of Li^+ ions during insertion/extraction, and thus facilitate performance at high rate. Moreover, the thin carbon layer, closely attached to the nanoparticles, can effectively prevent pulverization during cycling, leading to improved capacity retention and cycling life. Furthermore, the external carbon shell combined with interior interconnected nanostructure provides fast pathways for electron transport, enhancing the capacity at high rate.

3. Conclusions

In summary, we have demonstrated a facile and scalable approach for fabricating coral-like SnO_2/C composite electrodes through a top-down strategy followed by a sol–gel carbon coating method. Using the well-defined SnS_2 nanoflowers as a template, the resultant SnO_2/C composite displays a coral-like structure, composed of interconnected fine monocrystalline SnO_2 nanoparticles coated coherently by a uniform carbon layer. This electrode was then tested as anode for lithium batteries. Compared to the electrodes of the SnS_2 nanoflowers and interconnected SnO_2 nanoparticles, the optimized coral-like SnO_2/C composite shows significant improvement in both in rate capability and cycling reversibility. The enhanced performance is attributed to the coral-like framework, which provides more active reaction sites and shorter diffusion lengths and stabilizing effects due to facile strain relaxation between the interconnected nanoparticles. Moreover, the carbon layer coated on the SnO_2 nanoparticles can serve as buffering shells to accommodate volume variations, alleviate disintegration and pulverization during charge/discharge process, and provide integrated electron transport pathways, leading to fast reaction kinetics. As such, the optimized coral-like SnO_2/C is demonstrated as a promising anode material for advanced lithium ion batteries with high capacity and rate capability.

Experimental Section

Synthesis of coral-like SnO_2/C nanoparticles Composite Materials

In a typical experiment, $SnCl_4{\cdot}5\,H_2O$ (0.54 g) and thioacetamide (TAA) (0.49 g) were dissolved into 30 mL isopropyl alcohol. After stirring for half an hour, the solution was transferred into a Teflon-lined autoclave and heated at 180 °C for 24 h. After the autoclave was allowed to cool to room temperature, the precipitates of gold-coloured product (SnS_2 nanoflowers) were collected by centrifuge and rinsed with deionized water and alcohol several times separately. Finally, coral-like SnO_2 was obtained by annealing SnS_2 nanoflowers in air at 600 °C for 2 h with a heating rate of 2 °C min^{-1}.

To fabricate carbon-modified composite nanoparticles, dopamine (DPA) was used as carbon source. Typically, 100 mg coral-like SnO_2 was added into a solution containing 2 $mg\,mL^{-1}$ DPA and 10 mM 2-amino-2-hydroxymethyl- propane-1, 3-diol (TRIS) in ice water bath. After sonication for 5 min, the mixture was stirred continuously for about 6 h. Then the resultant precipitate was collected by centrifugation and washed with deionized water and absolute ethanol for several times and dried at 70 °C. Afterwards, the as-prepared SnO_2/Poly-DPA was carbonized under N_2 atmosphere at 600 °C for 2 h with a heating rate of 2 °C min^{-1}.

Characterization

The crystallographic structures of all of these three samples were characterized by Rigaku MiniFlex X-ray diffraction (XRD) measurement with Cu Kα radiation in a 2θ ranging from 10° to 90° at room temperature. The microstructure, morphology and energy-dispersive spectroscopy (EDS) were characterized by a FEI Quanta 3D FEG field emission scanning electron microscopy (FESEM). Brunauer–Emmet–Teller (BET) surface areas were determined by using Altamira AMI-200 system to investigate the adsorption of nitrogen. X-ray photoelectron spectroscopy (XPS) was carried out by an AXIS165 spectrometer using a twin-anode Al Kα (1486.6 eV) X-ray source with the charge neutralization function being turned on. Transmission electron microscopic (TEM) images, high-resolution transmission electron microscopic (HRTEM) images and selected area electron diffraction (SAED) were recorded by using a JEOL HRTEM (JEM-1400 electron microscope) with an acceleration voltage of 120 kV. TG were performed on a SII STA7300 analyzer at a heating rate of 2 °C min^{-1} in air.

Electrochemical Measurements

The anode material was assembled into CR2032-type coins in the glove-box filled with pure argon gas, using lithium foil as the counter electrode and celgard-2320 membrane as separator. The electrolyte was 1 M $LiPF_6$ dissolved in ethylene carbonate (EC), dimethyl carbonate (DMC) and diethylcarbonate (DEC) at a volumetric ratio of 1:1:1.The anode was composed of the as-prepared tin-based material (SnS_2 nanoflowers, SnO_2 interconnected particles or coral-like SnO_2/C) and carbon black as well as sodium alginate binder mixed at a weight ratio of 7:2:1 in deionized water followed by drying at 70 °C for 12 h. The assembled coins were aged for 24 h before electrochemical measurements to ensure full filtration of the electrolyte into the anode electrode's material. Galvanostatic charge/discharge measurements were performed using in a voltage range of 0.01–2.0 V (versus Li^+/Li) with an eight-channel battery analyzer (MTI Corporation). Cyclic voltammetry (CV) measurements were performed with an electrochemical workstation (CHI 6504C) at a scanning rate of 0.1 $mV s^{-1}$. The AC-impedance spectra were tested by applying an AC potential of 5 mV amplitude in the frequency range from 0.01 to 100 kHz with CHI 6504C.

Acknowledgements

This work is supported by REA (Research Enhancement Awards) and RAP (Research Awards Program) sponsored by LaSPACE. The authors would like to thank Mr. Zi Wang and Professor James Spivey in the department of chemical engineering at Louisiana State University (LSU) for their help with BET analysis. The authors also acknowledge LSU IAM Shared Instrumentation Facility (SIF) at LSU for using XRD, SEM, TEM, and XPS.

Keywords: anodes · composite electrodes · lithium-ion batteries · SnO_2/C core–shell materials · template synthesis

[1] J. M. Tarascon, M. Armand, *Nature* **2001**, *414*, 359 – 367.
[2] Y. M. Chiang, *Science* **2010**, *330*, 1485 – 1486.
[3] D. Butler, *Nature* **2007**, *445*, 586 – 588.
[4] X. D. Cui, W. W. Xu, Z. Q. Xie, Y. Wang, *J. Mater. Chem. A* **2016**, *4*, 1908 – 1914.
[5] B. Dunn, H. Kamath, J. M. Tarascon, *Science* **2011**, *334*, 928 – 935.
[6] A. Yoshino, *Angew. Chem. Int. Ed.* **2012**, *51*, 5798 – 5800; *Angew. Chem.* **2012**, *124*, 5898 – 5900.
[7] F. Y. Cheng, J. Liang, Z. L. Tao, J. Chen, *Adv. Mater.* **2011**, *23*, 1695 – 1715.
[8] J. B. Goodenough, K. Youngsik, *Chem. Mater.* **2010**, *22*, 587 – 603.
[9] M. Armand, J. M. Tarascon, *Nature* **2008**, *451*, 652 – 657.
[10] J. Lu, C. Y. Nan, L. H. Li, Q. Peng, Y. D. Li, *Nano Res.* **2013**, *6*, 55 – 64.
[11] T. Mommaa, N. Shiraishia, A. Yoshizawaa, T. Osakaa, A. Gedankenb, J. Zhub, L. Sominskib, *J. Power Sources* **2001**, *97*, 198 – 200.
[12] T. J. Kim, C. Kim, D. Son, M. Choi, B. Park, *J. Power Sources* **2007**, *167*, 529 – 535.
[13] K. Chang, Z. Wang, G. C. Huang, H. Li, W. X. Chen, J. Y. Lee, *J. Power Sources* **2012**, *201*, 259 – 266.
[14] C. X. Zhai, N. Du, H. Z. D. Yang, *Chem. Commun.* **2011**, *47*, 1270 – 1272.
[15] L. Q. Mai, L. Xu, C. H. Han, X. Xu, Y. Z. Luo, S. Y. Zhao, Y. L. Zhao, *Nano Lett.* **2010**, *10*, 4750 – 4755.
[16] C. H. Jiang, E. Hosono, H. S. Zhou, *Nano Today* **2006**, *1*, 28 – 33.
[17] L. Q. Mai, F. Yang, Y. L. Zhao, X. Xu, L. Xu, Y. Z. Luo, *Nat. Commun.* **2011**, *2*, 381.
[18] C. X. Zhai, N. Du, H. Zhang, J. X. Yu, D. R. Yang, *ACS Appl. Mater. Interfaces* **2011**, *3*, 4067 – 4074.
[19] X. J. Hou, X. F. Wang, B. Liu, Q. Q. Wang, Z. R. Wang, D. Chen, G. Z. Shen, *ChemElectroChem.* **2014**, *1*, 108 – 115.
[20] A. S. Aricò, P. Bruce, B. Scrosati, J. M. Tarascon, W. V. Schalkwijk, *Nat. Mater.* **2005**, *4*, 366 – 377.
[21] W. Shi, B. G. Lu, *Electrochim. Acta* **2014**, *133*, 247 – 253.
[22] W. W. Xu, Z. Q. Xie, X. D. Cui, K. N. Zhao, L. Zhang, G. Dietrich, K. M. Dooley, Y. Wang, *ACS Appl. Mater. Interfaces* **2015**, *7*, 22533 – 22541.
[23] Q. Q. Zhang, R. Li, M. M. Zhang, B. L. Zhang, X. L. Gou, *Electrochim. Acta* **2014**, *115*, 425 – 433.
[24] R. T. Huang, L. J. Wang, Q. Zhang, Z. W. Chen, Z. Li, D. Y. Pan, B. Zhao, M. H. Wu, C. M. L. Wu, C. H. Shek, *ACS Nano* **2015**, *9*, 11351 – 11361.
[25] Y. F. Dong, Z. B. Zhao, Z. Y. Wang, Y. Liu, X. Z. Wang, J. S. Qiu, *ACS Appl. Mater. Interfaces* **2015**, *7*, 2444 – 2451.
[26] L. Zhang, K. N. Zhao, W. W. Xu, Y. F. Dong, R. Xia, F. N. Liu, L. He, Q. L. Wei, M. Y. Yan, L. Q. Mai, *Phys. Chem. Chem. Phys.* **2015**, *17*, 7619 – 7623.
[27] C. Wang, G. H. Du, K. Ståhl, H. X. Huang, Y. J. Zhong, J. Z. Jiang, *J. Phys. Chem. C* **2012**, *116*, 4000 – 4011.
[28] V. Etacheri, G. A. Seisenbaeva, J. Caruthers, G. Daniel, J. M. Nedelec, V. G. Kessler, V. G. Pol, *Adv. Energy Mater.* **2015**, *5*, 1401289.
[29] H. N. Ma, J. He, D. B. Xiong, J. S. Wu, Q. Q. Li, V. Dravid, Y. F. Zhao, *ACS Appl. Mater. Interfaces* **2016**, *8*, 1992 – 2000.
[30] Y. F. Zhao, W. Ran, J. He, Y. Z. Huang, Z. F. Liu, W. Liu, Y. F. Tang, L. Zhang, D. W. Gao, F. M. Gao, *Small* **2015**, *11*, 1310 – 1319.
[31] Y. F. Zhao, W. Ran, D. B. Xiong, L. Zhang, J. Xu, F. M. Gao, *Mater. Lett.* **2014**, *118*, 80 – 83.
[32] W. W. Xu, K. N. Zhao, C. J. Niu, L. Zhang, Z. Y. Cai, C. H. Han, L. He, T. Shen, M. Y. Yan, L. B. Qu, L. Q. Mai, *Nano Energy* **2014**, *8*, 196 – 204.
[33] A. Bhaskara, M. Deepab, T. N. Rao, *Electrochim. Acta* **2015**, *184*, 239 – 249.
[34] Z. Y. Cai, L. Xu, M. Y. Yan, C. H. Han, L. He, K. M. Hercule, C. J. Niu, Z. F. Yuan, W. W. Xu, L. B. Qu, K. N. Zhao, L. Q. Mai, *Nano Lett.* **2015**, *15*, 738 – 744.
[35] C. Lei, F. Han, D. Li, W. C. Li, Q. Sun, X. Q. Zhang, A. H. Lu, *Nanoscale* **2013**, *5*, 1168 – 1175.
[36] H. S. Li, L. F. Shen, K. B. Yin, J. Ji, J. Wang, X. Y. Wang, X. G. Zhang, *J. Mater. Chem. A* **2013**, *1*, 7270 – 7276.
[37] M. Sathish, S. Mitani, T. Tomai, I. Honma, *J. Phys. Chem. C* **2012**, *116*, 12475 – 12481.
[38] W. W. Xu, K. N. Zhao, L. Zhang, Z. Q. Xie, Y. Wang, *J. Alloys Compd.* **2016**, *654*, 357 – 362.
[39] L. S. Zhang, Y. P. Huang, Y. F. Zhang, W. Fan, T. X. Liu, *ACS Appl. Mater. Interfaces* **2015**, *7*, 27823 – 27830.
[40] K. N. Zhao, L. Zhang, R. Xia, Y. F. Dong, W. W. Xu, C. J. Niu, L. He, M. Y. Yan, L. B. Qu, L. Q. Mai, *Small* **2015**, *12*, 588 – 594.
[41] R. Z. Hu, Y. P. Ouyang, D. C. Chen, H. Wang, Y. Chen, M. Zhu, M. L. Liu, *Acta Mater.* **2016**, *109*, 248 – 258.
[42] R. Z. Hu, D. C. Chen, G. Waller, Y. P. Ouyang, Y. Chen, B. Zhao, B. Rainwater, C. H. Yang, M. Zhu, M. L. Liu, *Energy Environ. Sci.* **2016**, *9*, 595 – 603.
[43] W. W. Xu, Z. Q. Xie, X. D. Cui, K. N. Zhao, L. Zhang, L. Q. Mai, Y. Wang, *J. Mater. Chem. A* **2016**, *4*, 3735 – 3742.

Manuscript received: March 10, 2016
Accepted Article published: April 28, 2016
Final Article published: ■■ ■■, 2016

*W. Xu, X. Cui, Z. Xie, G. Dietrich, Y. Wang**

■■ – ■■

Three-Dimensional Coral-Like Structure Constructed of Carbon-Coated Interconnected Monocrystalline SnO_2 Nanoparticles with Improved Lithium-Storage Properties

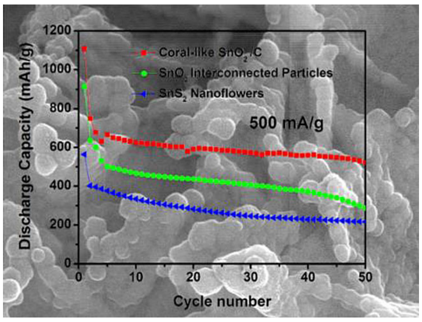

Shape matters: Coral-like SnO_2/C composite electrodes, fabricated through a top-down strategy followed by a sol–gel method of carbon coating, are compared to electrodes of SnS_2 nanoflowers and interconnected SnO_2 nanoparticles. The optimized coral-like SnO_2/C composite shows significant improvements in electrochemical performance, especially in terms of the rate capability and cycling reversibility.